Physiological
Measurement

PAPER • OPEN ACCESS

Quantification of pendelluft in electrical impedance tomography data: opening pandora's box? a literature review of analytical methods

To cite this article: Annemijn H Jonkman *et al* 2026 *Physiol. Meas.* **47** 075003

View the article online for updates and enhancements.

You may also like

- Flow transport and gas mixing during invasive high frequency oscillatory ventilation
Mohammed Alzahrany, Arindam Banerjee and Gary Salzman
- Large eddy simulation of high frequency oscillating flow in an asymmetric branching airway model
Martin A. Nagels and John E. Cater
- Fraction of reverse impedance change (FRIC): a quantitative electrical impedance tomography measure of intrapulmonary pendelluft
Andy Adler, Tobias Becher, Claas Händel et al.

This content was downloaded from IP address 192.167.211.143 on 27/10/2026 at 13:48

Physiological Measurement

IPEM Institute of Physics and Engineering in Medicine

Check for updates

PAPER

Quantification of pendelluft in electrical impedance tomography data: opening pandora's box? a literature review of analytical methods

Annemijn H Jonkman[1,*], **Juliette E Francovich**[1], **Anne Lotte Kuiper**[1], **Diederik Gommers**[1], **Gaetano Scaramuzzo**[2,3] **and Peter Somhorst**[1]

[1] Department of Adult Intensive Care, Erasmus MC, Rotterdam, The Netherlands
[2] Department of Translational Medicine, University of Ferrara, Ferrara, Italy
[3] Intensive Care Unit, Department of Emergency, Sant'Anna University Hospital, Ferrara, Italy
[*] Author to whom any correspondence should be addressed.

E-mail: a.jonkman@erasmusmc.nl

Keywords: pendelluft, electrical impedance tomography, preprocessing, quantification methods, mechanical ventilation

Supplementary material for this article is available online

OPEN ACCESS

RECEIVED
19 December 2025

REVISED
30 March 2026

ACCEPTED FOR PUBLICATION
15 June 2026

PUBLISHED
6 July 2026

Original content from this work may be used under the terms of the Creative Commons Attribution 4.0 licence.

Any further distribution of this work must maintain attribution to the author(s) and the title of the work, journal citation and DOI.

Abstract

Introduction. Pendelluft, i.e. the movement of air between different lung regions, has been associated with lung injury and ventilation inefficiencies in mechanically ventilated patients. Electrical impedance tomography (EIT) is the only bedside technology for real-time imaging of pendelluft. However, no universal method exists for measuring and quantifying pendelluft on EIT data. This review aims to evaluate and summarize the methods used to quantify pendelluft, with a focus on EIT analysis techniques. *Approach.* A search was conducted in three databases: Embase, Web of Science and Medline, using predefined search criteria. Steps for preprocessing and computation of pendelluft were identified. Calculation steps were standardized to enable comparison across studies, and the methods were applied to EIT data to visualize the differences between them. *Main results.* 19 studies were included, with six unique methods for quantifying pendelluft on EIT data. The methods have some similarities, but mostly quantify pendelluft differently. Preprocessing methods vary greatly among the methods. These methodological differences are reflected in the variability of results when applying the methods to patient data. *Significance.* Different methods for quantifying pendelluft with EIT exist, which differ considerably in pendelluft quantification and in EIT preprocessing. Further development and consensus on quantification techniques and standardized reporting are necessary for advancing research into pendelluft and its impact, and improving clinical applicability. This highlights a promising research avenue for EIT as bedside modality for monitoring the impact of spontaneous breathing on regional lung mechanics.

1. Introduction

Pendelluft refers to the redistribution of air between lung regions (Otis *et al* 1956, Maloney *et al* 1961, Coppadoro *et al* 2020b). It was first described in a report from observations during open thoracic surgeries as early as 1909, where dyspneic breathing was attributed to pendelluft (Brauer 1909), and has since been observed in mechanically ventilated patients with obstructive lung diseases (Vyshedskiy and Murphy 2012), flail chest (Harada *et al* 1983), and acute respiratory distress syndrome (ARDS) (Lin *et al* 2023). Although often associated with spontaneous breathing such as during assisted ventilation, pendelluft can also occur with passive controlled ventilation (Santini *et al* 2019). The development of pendelluft is driven by pressure gradients across lung regions, which can arise from lung heterogeneity and/or from the distribution of the generated negative pressure throughout the lung parenchyma. Parenchymal

© 2026 The Author(s). Published on behalf of Institute of Physics and Engineering in Medicine by IOP Publishing Ltd

heterogeneity might determine differences in airway opening pressures, airway resistance and lung compliance, which can lead to inhomogeneities in time constants. In addition, the negative pressure generated by respiratory muscles, in particular the diaphragm, might not be uniformly distributed, resulting in a pressure gradient that drives air from ventral to dorsal lung regions (Yoshida *et al* 2013, 2017, Coppadoro *et al* 2020b).

A variety of techniques have been used to measure pendelluft, including positron imaging (Tsuzaki *et al* 1993), multi-channel lung sound analysis (Vyshedskiy and Murphy 2012), darkfield microscopy (Tabuchi *et al* 2016), and dynamic computed tomography (Yoshida *et al* 2013). These techniques are not practical for bedside monitoring, which limits their clinical applicability in mechanically ventilated patients. Electrical impedance tomography (EIT) is the only noninvasive bedside technology that enables real-time assessment of regional ventilation distribution (Frerichs *et al* 2017). The first description of pendelluft using EIT was in a porcine model with injured lungs (Yoshida *et al* 2013), showing transient and potentially injurious regional (dorsal) lung stretch in response to strong diaphragm contractions, despite 'lung-protective' ventilation with low tidal volume settings. This triggered the interest in studying pendelluft as potential indicator of risk factors for worsening lung injury and inflammation in patients with high respiratory drive (i.e. patient self-induced lung injury), particularly in patients transitioning from controlled to assisted ventilation where excessive and/or asynchronous breathing efforts are common (Cornejo *et al* 2022, Lin *et al* 2023, Bassi *et al* 2025).

Although the physiological meaning of the phenomenon (i.e. the redistribution of air between lung regions) is rather simple, the EIT-based mathematical definition and evaluation is not straightforward, since different considerations should be made on signal preprocessing and analyses. With the increased interest in pendelluft monitoring with EIT, different definitions and quantification methods have appeared in literature (Scaramuzzo *et al* 2024), making it difficult to compare and reproduce studies and to evaluate the clinical impact of pendelluft. In this review, we summarize and evaluate current unique methods used to define, measure and quantify pendelluft with EIT. Because signal preprocessing steps directly affect subsequent parameter computations, we examine both EIT preprocessing and the computational methods used to derive pendelluft. We conclude by discussing the advantages and limitations of the methods, aiming to contribute to a clearer understanding of the complex quantification of the pendelluft phenomenon.

2. Approach

The Embase database, Medline, and Web of Science were searched from inception to 26 November 2024, for relevant articles. The search combined the terms 'Pendelluft' and 'Electrical Impedance Tomography'. For the full search string, see the Supplemental file. Only articles accessible through the Erasmus MC library and published in English were included. After deleting duplicates, the title and abstract of the articles were screened (ALK). Subsequently, the full text was read to assess eligibility (ALK, AHJ, PS). Studies were included (a) if they measured pendelluft using EIT or (b) when they described methodologies for measuring pendelluft with EIT. Eligible studies also had to provide a quantification of pendelluft and include a description of the signal analysis techniques applied to the EIT data. Conference abstracts and editorials were excluded. Additional articles were identified via cross-referencing the eligible studies.

All signal preprocessing steps were identified for each pendelluft computation method. The remaining pendelluft calculation steps were identified and parameters were standardized (see below) to facilitate method comparisons. Initial extraction of information was done by ALK and by AHJ and confirmed by JEF and PS. Authors of the studies were consulted for additional clarifications, if needed. To illustrate the implications of the different methods, the algorithms were reproduced in Python (version 3.13.5) and applied to data of a representative patient with hypoxemic failure on assisted ventilation.

2.1. Standardized terminology

To facilitate the comparison across different methods (see figure 1), we standardized terminology for breath-related impedance differences as follows:

1) The start (t_s) and end (t_e) of global inspiration are based on the extreme values in the global impedance signal (i.e. the sum of all pixels in the EIT image) or in the functional impedance signal (i.e. the sum of those pixels that are included in the functional lung space), depending on whether the method uses functional lung segmentation in the preprocessing. The *global TIV* or *functional TIV* refers to the difference in global or functional impedance between t_s and t_e.

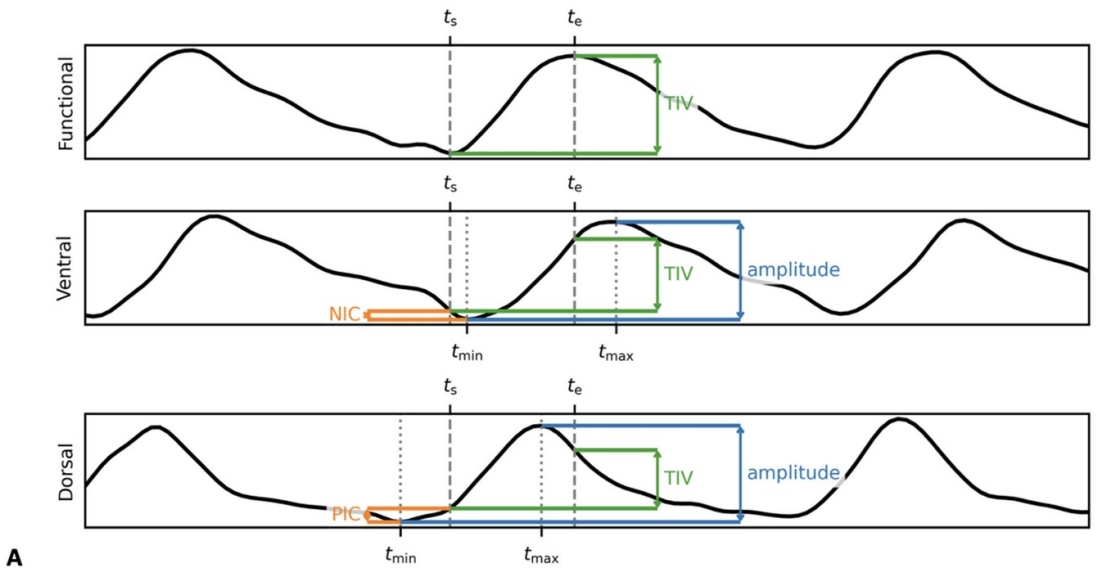

Method	Simplified approximation
Coppadoro	$\text{Regional pendelluft} \approx \frac{\text{NIC}_{\text{regional}} \text{ or } \text{PIC}_{\text{regional}}}{\text{TIV}_{\text{functional}}}$
Sang	$\text{Pixel pendelluft} \approx \frac{\text{amplitude}_{\text{pixel}} - \text{TIV}_{\text{pixel}}}{\text{TIV}_{\text{functional}}}$
Menga	$\text{Pixel pendelluft} \approx \frac{\text{amplitude}_{\text{pixel}} - \text{TIV}_{\text{pixel}}}{\text{amplitude}_{\text{functional}}}$
Adler	$\text{Pixel pendelluft} \approx \frac{\text{NIC}_{\text{pixel}}}{\text{amplitude}_{\text{pixel}} + \text{NIC}_{\text{pixel}}}$

B

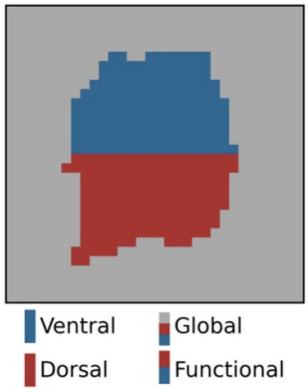

Figure 1. (A) Standardized terminology of impedance-related parameters. The start (t_s) and end (t_e) of functional (or global) inspiration are based on the extreme values in the functional (or global) impedance signal. The *global TIV* or *functional TIV* thus refers to the difference in global or functional impedance between t_s and t_e. The *pixel TIV* or *regional TIV* (e.g. ventral TIV) is the change in pixel or regional impedance between t_s and t_e. The *pixel amplitude* or *regional amplitude* refers to the difference between the minimum (at t_{min}) and maximum (at t_{max}) values in a pixel or region during a breath cycle. NIC is the negative impedance change during global or functional inspiration and PIC is the positive impedance change during global or functional inspiration. (B) Simplified approximate equations based on the standardized terminology of four of the presented algorithms. Cornejo's and Santini's algorithms are not included here since they use different approaches that cannot be simplified using the terminology in figure (A). (C) Region of interests (ROI): pixels inside the global ROI (all pixels), functional ROI (respiration-related), ventral ROI (parts of functional ROI that are in the upper 16 rows) and dorsal ROI (parts of functional ROI that are in the lower 16 rows). Resulting impedance signals are the sum of the impedances of pixels inside the ROI.

2) The *pixel TIV* or *regional TIV* (e.g. ventral TIV) is defined as the change in pixel or regional impedance between t_s and t_e (equation 1).

3) The *pixel amplitude* or *regional amplitude* refers to the difference between the minimum and maximum values in a pixel or region during a breath cycle (equation 2). The timing of the minimum and maximum are defined as t_{min} and t_{max}, respectively.

4) The *global* or *functional amplitude* is defined as the sum of all pixel or regional amplitude values. By definition, the amplitude is equal to (with no pendelluft) or greater than (in case of pendelluft) the TIV.

5) Following Adler *et al* (2024), we define the negative impedance change (NIC) of a pixel or region as the decrease in impedance during the global or functional inspiration phase. Likewise, we define the positive impedance change (PIC) of a pixel or region as the increase in impedance during the global or functional expiration phase.

$$\mathrm{TIV}_{i,n} = \Delta Z_{i,n}(t_e) - \Delta Z_{i,n}(t_s) \quad (1)$$

where $\mathrm{TIV}_{i,n}$ is the TIV of pixel or region i, of breath n. $\Delta Z_{i,n}(t_e)$ and $\Delta Z_{i,n}(t_s)$ are the relative ΔZ of pixel i at the global time points, with t_s and t_e the start and end of global inspiration, for breath n.

$$\mathrm{amplitude}_{i,n} = \Delta Z_{i,n}(t_{max}) - \Delta Z_{i,n}(t_{min}) \quad (2)$$

where $\mathrm{amplitude}_{i,n}$ is the amplitude of pixel or region i, of breath n. $\Delta Z_{i,n}(t_{max})$ and $\Delta Z_{i,n}(t_{min})$ are the relative ΔZ of pixel i at the time points of maximum and minimum pixel or regional impedance, for breath n.

In respiratory physiology literature, the terms dependent and non-dependent are used to indicate a gravity-dependency; for instance, of compliance in different lung regions. These terms have become somewhat synonymous with ventral and dorsal regions, since generally ventilated patients are in the supine position. Pendelluft directionality, however, seems to be not mainly a gravity-dependent phenomenon, but an anatomical phenomenon, in particular during patient breathing efforts: the diaphragm is shaped such that the largest negative pressure is generated toward the dorsal areas of the thorax. Indeed, ventilation distribution can shift during prone position in patients with breathing efforts (Grieco *et al* 2023) but we found no indication that the directionality of pendelluft depends on body position. Because all algorithms that use regionality were developed for pendelluft quantification during patient breathing efforts, we use the anatomical indicators ventral and dorsal in the description of their algorithms.

3. Main Results

3.1. Study selection

Of the 253 studies identified by the search, 19 were found to meet the inclusion criteria (see figure 2 for PRISMA diagram). Of these 19 studies, six presented unique methods for pendelluft quantification. One was applied to passive patients while five were used to measure pendelluft in spontaneously breathing patients.

3.2. Study characteristics

Table 1 shows a summary of the characteristics of the included articles. These include the studies that described a unique pendelluft computation method, as well as studies that adopted these methods.

3.3. EIT signal processing before pendelluft calculation

EIT signal processing generally consists of three steps: 1. filtering the data to attenuate the cardiac signal, other noise and artifacts, 2. selecting the functional lung space, and 3. selecting regions of interest (ROI) (Scaramuzzo *et al* 2024).

The analyzed studies acquired the EIT signal using a frame rate between 20 Hz and 50 Hz. As concerns filtering, multiple studies used low-pass filtering, which is a classical and simple method for cardiac filtering and/or to remove noise (Sang *et al* 2020, Jiang *et al* 2023, Lin *et al* 2023, Adler *et al* 2024, Heines *et al* 2024, Liu *et al* 2024). Others used or suggested breath averaging to enhance signal quality (Coppadoro *et al* 2020a, Menga *et al* 2023, Adler *et al* 2024) via event-triggering (e.g. based on identification of positive flow (Coppadoro *et al* 2020a) or the esophageal pressure signal (Menga *et al* 2023)). One study used a smoothing window to minimize baseline drift (Cornejo *et al* 2022). Menga *et al* (2023), Grieco *et al* (2023) and Bello *et al* (2024) used the processed signal of the EIT-device (FluxMed®). In contrast, Santini *et al* (2019) applied their pendelluft calculation to unprocessed EIT data.

Functional lung space selection was not consistently used or mentioned. Multiple studies used the lung contouring algorithm of the LuMon™ system (Sentec, Switserland) that is based on the patient's anthropometric characteristics (Grieco *et al* 2023, Menga *et al* 2023, Bello *et al* 2024). Another common method is to apply a threshold at a fraction of the maximum pixel TIV to determine the functional lung image (Frerichs *et al* 2017), which was done by Jiang *et al* (2023) and Adler *et al* (2024). Similarly, Sang *et al* (2020) used a threshold at a fraction of the maximum standard deviation of the pixel signal, as previously described (Zhao *et al* 2018).

Finally, the selection of ROIs also varied. Both Coppadoro *et al* (2020b) and Cornejo *et al* (2022) divided the whole EIT image into four equally-sized horizontal regions (layers 1–4 from most ventral

Table 1. Characteristics of studies presenting a unique method for pendelluft computation.

Author	Patient population	Cardiac filtering	Additional filtering	Functional image selection	Selection ROIs	Pendelluft unit	Pendelluft definition	Used by
				Controlled ventilation				
Santini *et al* 2019	10 ARDS patients on VCV	—	—	—	Pixel-based	% of VT, or mL	During an inspiratory hold, the sum of the absolute impedance difference between the zero flow time point and 3 s after the start of the hold, as a percentage of tidal volume.	—
				Assisted ventilation				
Coppadoro *et al* 2020b	20 difficult-to-wean patients on PSV	Breath averaging via event-triggering (identification based on flow)	—	—	4 regions of equal thickness, from ventral to dorsal	mL	The sum of the NIC and the PIC across all regions of interest, converted to mL.	Lin *et al* (2023), Lee *et al* (2024)
Sang *et al* 2020	6 patients: 2 with flail chest without ventilation support, 2 with ARDS on VCV and 2 with obstructive lung disease on ACV	Low-pass filter at 0.67 Hz	—	Thresholding based on fraction of maximum pixel standard deviation (20%[1])	Pixel-based	% of TIV	The difference between the pixel TIV and the pixel amplitude, as a percentage of the global TIV.	Liu *et al* (2024), Jiang *et al* (2023), Heines *et al* (2024), Xiao *et al* (2024), Xiao *et al* (2022), Chi *et al* (2022), Wang *et al* (2023), (Arellano *et al* 2023)
Cornejo *et al* 2022	24 ARDS patients transitioning from controlled to assisted ventilation	—	Smoothing window to minimize drift	Lung contouring of the Enlight system (mesh based on sex, thoracic perimeter and height) Thresholding based on fraction of maximum pixel TIV (typically <9%)[1]	2 regions: ventral and dorsal	% of TIV, or % of VT (negative values)	The average difference between the normalized ventral and dorsal lung region impedance signals during inspiration (only the negative portion), as a percentage of normalized tidal volume.	

(Continued.)

Table 1. (Continued.)

Author	Patient population	Cardiac filtering	Additional filtering	Functional image selection	Selection ROIs	Pendelluft unit	Pendelluft definition	Used by
Menga *et al* 2023	15 hypoxemic patients with noninvasive ventilator modes: NIV and CPAP	Breath-averaging via event-triggering (based on esophageal pressure signal)	—	Lung contouring based on anthropometric data (LuMon™ system)	Pixel-based	% of summed amplitude	The difference between the pixel TIV and pixel amplitude, as a percentage of the summed amplitude.	Grieco *et al* (2023), Bello *et al* (2024)
Adler *et al* 2024	1 ARDS patient on PSV	Breath averaging or bandpass filtering at heart rate	6th order Butterworth filter at 10 Hz	Thresholding based on fraction of maximum pixel TIV (10%[1])	Pixel-based	fraction or %	Fraction of impedance change in the reverse direction (FRIC), quantified as the NIC as fraction of the sum of the NIC and the pixel amplitude.	—

[1]Based on communication with author. Abbreviations: ACV, assist-control ventilation; PSV, pressure-support ventilation; ROIs, regions of interest; SBT, spontaneous breathing trial; VCV, volume-controlled ventilation; VT, tidal volume.

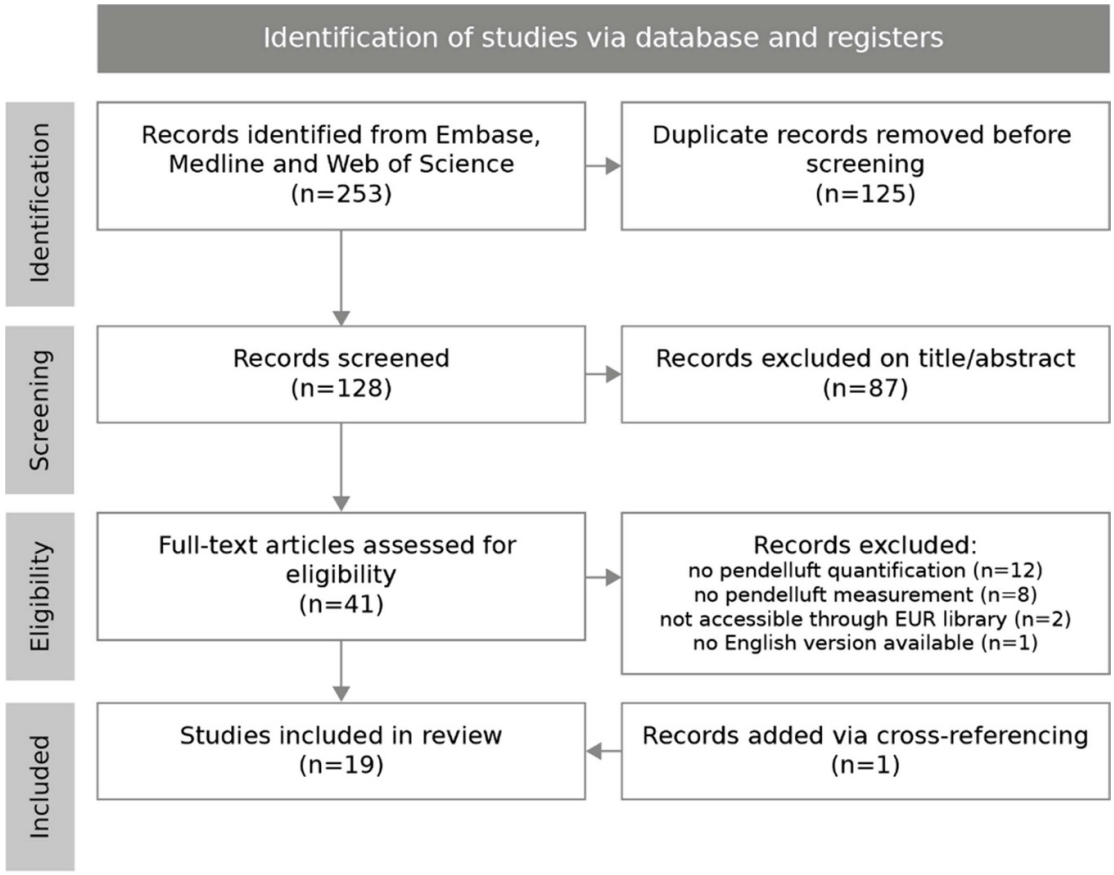

Figure 2. PRISMA diagram of identified and included studies. Abbreviations: EUR: Erasmus University Rotterdam.

to most dorsal), which were then combined into a ventral and dorsal lung region. Alternatively, studies present a pixel-by-pixel methodology, rather than dividing the lung into predefined regions (Santini *et al* 2019, Sang *et al* 2020, Chi *et al* 2022, Xiao *et al* 2022, Grieco *et al* 2023, Jiang *et al* 2023, Menga *et al* 2023, Wang *et al* 2023, Adler *et al* 2024, Bello *et al* 2024, Heines *et al* 2024, Liu *et al* 2024, Xiao *et al* 2024).

3.4. Pendelluft computation

The following equations described for each of the six unique methods are standardized for parameter terminology and might therefore differ textually (but not in computation) from the original articles. Preprocessing steps and a summarized description of pendelluft computation methods are provided in table 1. Figure 1(B) provides a summary of *simplified* approximate equations for pendelluft calculations based on the standardized terminology proposed in figure 1(A) for four of the algorithms.

Pendelluft has been expressed in different units, such as impedance amplitude, percentage, or milliliters (mL). Pendelluft amplitude can be converted to mL if the ventilator tidal volume is synchronized with EIT, given that changes in impedance correspond to changes in lung volume (Mauri *et al* 2016). A conversion factor is then computed as the ratio between global or functional TIV and tidal volume. The methods are reported in chronological order of publication.

3.4.1. Santini et al

Santini *et al* (2019) quantified pendelluft during an end-inspiratory hold in ten ARDS patients on protective volume-controlled ventilation. During the hold, t_{P_1} was identified as the time point corresponding to the first moment of negative or zero flow, and P_1 as the (airway or transpulmonary) pressure at that time. $t_{P_{plat}}$ was defined as 3 s after the start of the inspiratory hold, and P_{plat} was determined as the (airway or transpulmonary) pressure at that time. EIT images corresponding to t_{P_1} and $t_{P_{plat}}$ were selected and their absolute difference was calculated. Pendelluft was then calculated as the sum of the absolute impedance difference in each pixel (equation 3). The amplitude was converted to milliliters using a conversion factor derived from the previous unoccluded breath, or was expressed as percentage of the measured tidal volume.

$$\text{Pendelluft}_{\text{Santini}}\,(\text{mL}) = \sum_{i=1}^{1024} \left|\Delta Z_i\left(t_{P_1}\right) - \Delta Z_i\left(t_{P_{\text{plat}}}\right)\right| \cdot \text{conversion factor} \tag{3}$$

where $\Delta Z_i\left(t_{P_1}\right)$ and $\Delta Z_i\left(t_{P_{\text{plat}}}\right)$ represent the relative impedance values in the raw EIT signal per pixel i at t_{P_1} and $t_{P_{\text{plat}}}$ points.

3.4.2. Coppadoro et al

Coppadoro *et al* (2020b) quantified pendelluft in 20 patients who had failed a spontaneous breathing trial, by comparing global and regional impedance-time curves. Pendelluft was calculated as the sum of the NIC and PIC of each of four ROIs (NIC and PIC are mutually exclusive for each layer) (equation 4). Simultaneously, they defined ventral pendelluft as $\text{NIC}_{\text{dorsal}} + \text{PIC}_{\text{ventral}}$, and dorsal pendelluft as $\text{NIC}_{\text{ventral}} + \text{PIC}_{\text{dorsal}}$. Pendelluft values were converted into mL. Furthermore, the authors present a pixel-level pendelluft map for a functional lung space (their figure 5 (Coppadoro *et al* 2020b)) but no description is reported on how this was derived.

$$\text{Pendelluft}_{\text{Coppadoro}}\ (\text{mL}) = \sum_{i=\text{layer 1}}^{\text{layer 4}} (\text{NIC}_i + \text{PIC}_i) \cdot \text{conversion factor} \tag{4}$$

where NIC_i and PIC_i are the NIC and PIC for a layer, respectively.

3.4.3. Sang et al

Sang *et al* (2020) calculated pendelluft for data from six patient cases with flail chest, ARDS, or obstructive lung disease. They used a pixel-by-pixel approach where the functional TIV and the pixel TIV were determined for every breath. To obtain a pendelluft image per breath, the pendelluft amplitude was computed for each pixel as the difference between the pixel amplitude and the pixel TIV, divided by the functional TIV and expressed as percentage (equation 5). It thus represents a proportion of functional TIV that is attributable to pendelluft.

$$\text{Pendelluft}_{\text{Sang},i,n}\ (\%) = \frac{\text{amplitude}_{i,n} - \text{TIV}_{i,n}}{\text{functional TIV}_n} \cdot 100\% \tag{5}$$

where i represents a pixel and n the breath number.

The pendelluft amplitude map was averaged for the included breaths (equation 6), and can be summed over all pixels to obtain the total pendelluft amplitude (equation 7).

$$\text{Pendelluft}_{\text{Sang},i}\,(\%) = \frac{1}{N}\sum_{n=1}^{N} \left(\text{Pendelluft}_{\text{Sang},i,n}\right) \tag{6}$$

$$\text{Pendelluft}_{\text{Sang,total}}\,(\%) = \sum_{i=1}^{1024} \left(\text{Pendelluft}_{\text{Sang},i}\right). \tag{7}$$

3.4.4. Cornejo et al

Cornejo *et al* (2022) measured pendelluft in ARDS patients switching from controlled to assisted ventilation. The time points for start and end of inspiration were taken as the time points of the minimum ($t_{\text{min,layer 4}}$) and maximum ($t_{\text{max,layer 4}}$) values of the breath cycle in layer 4 (i.e. the most dorsal ROI and closest to the diaphragm). The ventral and dorsal impedance were both normalized per inspiratory cycle to a range of 0–1. The normalized signals were then subtracted (equation 8), yielding the normalized impedance difference between the two regions.

$$\Delta Z_{\text{norm,diff},n}\,(t) = \Delta Z_{\text{norm,ventral},n}\,(t) - \Delta Z_{\text{norm,dorsal},n}\,(t) \tag{8}$$

where $\Delta Z_{\text{norm,ventral},n}$ and $\Delta Z_{\text{norm,dorsal},n}$ are the normalized ΔZ for each of the two regions.

To obtain a pendelluft volume, the negative portion of the signal $\Delta Z_{\text{norm,diff},n}\,(t)$ during the inspiratory cycle is then averaged and expressed as percentage of TIV or tidal volume (by using a conversion factor between TIV and tidal volume) for a specific breath n, see equation 9.

$$\text{Pendelluft}_{\text{Cornejo},n}\,(\%) = \sum_{t=t_{\text{min,layer 4}}}^{t_{\text{max,layer 4}}} \Delta Z_{\text{norm,diff},n}\,(t) \cdot \frac{\Delta t}{T} \cdot \text{conversion factor} \tag{9}$$

where Δt is the stepsize between each time point and T is the number of timepoints between $t_{\text{min,layer 4}}$ and $t_{\text{max,layer 4}}$ (inclusive).

In case of pendelluft due to patient effort, the calculated value will be negative, as the ventral impedance signal lags behind the dorsal impedance signal. To calculate the total pendelluft magnitude, the average value over the breaths was taken. The frequency of pendelluft was expressed as the proportion of breath cycles presenting pendelluft amplitudes exceeding a certain cut-off point. These cut-off points were set at −15, −20 and −25% of the tidal volume (Cornejo *et al* 2022).

3.4.5. Menga et al

Menga *et al* (2023) studied respiratory physiology during helmet pressure support, continuous positive airway pressure and high-flow nasal oxygen using several parameters, including pendelluft. Their quantification method partly relies on the same principle as that of Sang *et al* (2020).

Pendelluft was quantified on an averaged EIT breath. Averaging was done by resampling and interpolating the EIT signal using the timing of a synchronized esophageal pressure waveform (i.e. a window of 1.5 s before and after the nadir in esophageal pressure was used). Pixel TIV and pixel amplitude were calculated for this averaged breath (see equations 3 and 4, with n now representing the average breath). The pendelluft amplitude was computed for each pixel as the difference between the pixel amplitude and the pixel TIV, divided by the functional amplitude (i.e. sum of included pixel amplitudes) and expressed as percentage (equation 10). It thus represents a proportion of summed amplitude that is attributable to pendelluft.

$$\text{Pendelluft}_{\text{Menga},i}\,(\%) = \frac{\text{amplitude}_i - \text{TIV}_i}{\sum_{i=1}^{1024}(\text{amplitude}_i)} \cdot 100\% \tag{10}$$

where i represents a pixel of the average breath.

The pendelluft amplitude map was summed over all pixels to obtain the total pendelluft amplitude (equation 11).

$$\text{Pendelluft}_{\text{Menga,total}}\,(\%) = \sum_{i=1}^{1024}\left(\text{Pendelluft}_{\text{Menga},i}\right). \tag{11}$$

3.4.6. Adler et al

Adler *et al* (2024) introduced the fraction of reverse impedance change (FRIC), and applied their method to the data of one ARDS patient. FRIC quantifies the percentage of air moving opposite to the expected direction during inspiration. First, t_s (i.e. inspiration onset on the global impedance curve) was determined based on the change in derivative of the global signal. The authors mention that if pixels started to inflate prior to t_s, the t_s was moved to an earlier point in time to capture all pendelluft; thus, t_s here corresponded to the earliest t_{min} among all pixels. It should be noted that, by definition, in case of pendelluft at least some pixels will inflate before the global t_s.

In case of a well-filtered signal, the calculation of the FRIC per pixel is equivalent to the NIC divided by the sum of pixel amplitude and NIC (equation 12). The total FRIC per breath is calculated similarly, summing the NIC and amplitude over all pixels first (equation 13) and then expressed as percentage. In case of a signal containing e.g. cardiovascular noise, the calculations are more complicated (see Supplemental file).

$$\text{Pendelluft}_{\text{Adler},i} = \frac{\text{NIC}_i}{\text{amplitude}_i + \text{NIC}_i} \tag{12}$$

where i represents a pixel.

$$\text{Pendelluft}_{\text{Adler,total}}\,(\%) = \frac{\sum_{i=1}^{1024}\text{NIC}_i}{\sum_{i=1}^{1024}\text{amplitude}_i + \sum_{i=1}^{1024}\text{NIC}_i} \cdot 100\% \tag{13}$$

where i represents a pixel.

3.5. Application to EIT data

To compare the results derived from the different methods, we applied the five methods suitable for pendelluft computation (*Coppadoro, Cornejo, Sang, Menga, Adler*) during assisted ventilation to two EIT recordings of a patient with hypoxemic respiratory failure ventilated in pressure support mode. For each method, the preprocessing as described in the original articles was used. However, Menga *et al* (2023)

Table 2. Pendelluft computations for two EIT recordings of the same patient during pressure support ventilation. EIT data was recorded with the Dräger Pulmovista 500 directly after switching from pressure control to pressure support mode (recording 1) and after approximately 4 h on pressure support mode (recording 2). Synchronized esophageal pressure signals were available, as required for the method of Menga *et al*. Ventilator settings were 15 cmH_2O pressure support over 15 cmH_2O PEEP, with average esophageal pressure swings of around 12 cmH_2O in both recordings.

Method (unit)	Coppadoro (mL)	Sang (% TIV)	Cornejo (% TIV)	Menga (% summed amplitude)	Adler (% FRIC)
Recording 1	2.8 (0.60% of TIV)	3.9	−4.0	4.7	6.2
Recording 2	4.4 (1.1% of TIV)	5.7	−4.9	9.5	12.1

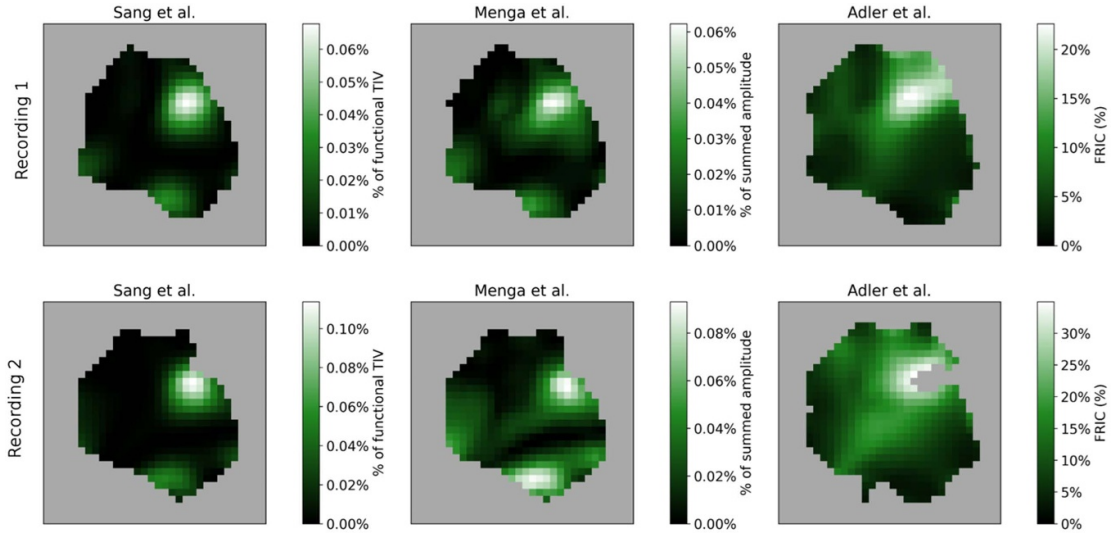

Figure 3. Pendelluft amplitude calculation for the different methods in a representative patient during two recordings (see table 2 and text for more details).

used data from the LuMon system (Sentec), which applies anatomical-based lung contouring that is specific for this device. We could not exactly reproduce this in our EIT data that was acquired with a different machine (Pulmovista 500, Dräger). As their pendelluft computation is most similar to the method of Sang *et al* (2020), we applied functional lung space selection of Sang *et al* (2020) prior to using Menga *et al* (2023) further preprocessing (i.e. breath averaging) and pendelluft computation.

Different pendelluft amplitudes were observed for each method (table 2). When comparing pendelluft values between the two EIT recordings, the direction of change for pendelluft was similar across methods, with larger values for methods of Coppadoro, Sang, Menga, and Adler, and more negative values for Cornejo's method (table 2). Pendelluft maps were created for methods of Sang *et al* (2020), Menga *et al* (2023) (when using lung space selection of Sang *et al* (2020)), and Adler *et al* (2024) (figure 3). No color maps were created for Coppadoro *et al* (2020b) as no information was provided on how to create these pixel maps, nor for Cornejo *et al* (2022) as individual pixels were not analyzed in their work. We can observe that the method from Adler *et al* (2024) detects pendelluft solely in the ventral lung regions, whereas Sang *et al* (2020) and Menga *et al* (2023) also detect pendelluft in the dorsal regions. Furthermore, functional lung space selection methods differ between methods, affecting the amount of included pixels in the analyses (supplemental figure 2). Regions of NIC can be removed from the lung contouring: due to the phase shift with pendelluft, pixel TIV or pixel standard deviation within pendelluft-associated regions can be below the applied thresholds for lung segmentation (see figure 3, upper right corner in recording 2).

4. Significance

We identified and summarized six unique methods for quantifying pendelluft with EIT. Although some methods share similar underlying principles, they differ considerably in how pendelluft is quantified and in their preprocessing methods. These methodological differences are reflected in the variability of results when applying the methods to example patient data.

4.1. Comparison and physiological meaning of quantification methods

Most methods are applicable to EIT data acquired during both controlled ventilation and spontaneous breathing. Only one (Santini *et al* (2019)) has been described exclusively in passive patients since it requires an inspiratory breath hold during controlled ventilation for pendelluft calculation. This limits the clinical applicability toward a continuous measurement, during different ventilator modes and with spontaneous breathing efforts. Moreover, from a physiological perspective, this method differs from the other methods, since it evaluates the redistribution of air during an inspiratory hold at the end of passive inspiration and not the redistribution of air during the active inspiration phase (Santini *et al* 2019). It is therefore not related to patient self-induced lung injury mechanisms, but mostly an indication of resistance and compliance heterogeneity.

The methods by Sang *et al* (2020) and Menga *et al* (2023) are most similar in terms of pendelluft computation beyond preprocessing, except for the denominator. Sang *et al* (2020) follows the 1956 description by Otis *et al* (1956), who calculated pendelluft as the difference in volume between the sum of the individual tidal volumes and the overall tidal volume, as a percentage of the effective tidal volume. In contrast, Menga *et al* (2023) measures pendelluft as percentage of the summed amplitude, representing the total air displacement in the lungs. Coppadoro *et al* (2020b) has a similar approach but computes pendelluft in mL which can be compared to the tidal volume and has more limited spatial resolution since it is based on ROI and not pixel values. Since, in the presence of pendelluft, the global TIV is smaller than the summed amplitude, the method of Sang *et al* (2020) should result in a larger pendelluft amplitude as compared to the method of Menga *et al* (2023) when applied to the same dataset. If not, differences must be explained by different preprocessing steps. In our example (see Results), we applied a similar lung segmentation for both methods. Therefore, the difference likely originates from breath averaging with Menga's method (Menga *et al* 2023) that is based on esophageal pressure timings, versus low-pass filtering with Sang *et al* (2020). Indeed, when applying the same preprocessing steps for both methods, the pendelluft amplitude with Sang's method was higher than with Menga's method (see Supplemental file), as expected.

It is essential to differentiate pendelluft from other forms of regional ventilation variability, such as regional ventilation delay, where a region inflates and deflates at the same time but relatively slowly compared to the global signal. Cornejo *et al* (2022) incorporated the entire EIT signal dynamics rather than looking at amplitudes. As a result, this method does not solely capture pendelluft, but also other phenomena such as regional changes in compliance during inspiration (as can be quantified using intratidal gas distribution curves (Lowhagen *et al* 2010)) and delayed inflation due to regional airway closure. These phenomena are not generally considered pendelluft and are not included in pendelluft calculation by other methods. Adler *et al* (2024) argued that phase-based techniques, like those by Chi *et al* (2022) and Liu *et al* (2024) (who adopted the method by Sang *et al* (2020)) may erroneously attribute timing variability from non-pendelluft factors to pendelluft, as the phase difference reflects a lagging regional response rather than actual air redistribution (Chi *et al* 2022, Adler *et al* 2024, Liu *et al* 2024). However, the solution proposed by Adler *et al* (2024) does not solve this issue, as their approach is very similar: i.e. comparing a measure of reverse flow to the total amplitude or TIV, without considering time-based properties. Furthermore, by quantifying only reverse-flow, Adler's algorithm (Adler *et al* 2024) detects pendelluft solely in regions from which air is withdrawn (i.e. ventral pixels, see also figure 3), not in those to which it is redistributed. The latter is of clinical interest as those lung regions that are receiving the redistributed volume may be at risk for high lung strain, depending on both the amount of redistributed volume and the size of the receiving region.

4.2. EIT acquisition and preprocessing

Preprocessing steps—consisting of filtering, breath detection, lung segmentation and/or ROI selection—differed among methods. Both Coppadoro *et al* (2020b) and Cornejo *et al* (2022) apply ROI selection and/or functional lung segmentation prior to filtering. Filtering is, however, recommended as first step (Scaramuzzo *et al* 2024) as it might influence the resulting impedance summation to ROIs or the functional lung region.

Several studies used low-pass filters to minimize cardiovascular interference, but this can result in the loss of harmonics that carry important respiratory signal details (Wisse *et al* 2024b). Standard low-pass filtering or otherwise excessive filtering can alter the amplitude and timing of the signal (Wisse *et al* 2024b)—and thus the location of t_s, t_e, t_{min} and t_{max}, and amplitude, TIV and ultimately pendelluft computation. Coppadoro *et al* (2020a) showed that event-triggered breath averaging (based on flow) could mitigate the phase distortion caused by low-pass filtering. However, breath-averaging is only suitable for patients with stable breathing patterns, which may not be the case in patients with pendelluft.

Advanced filtering techniques, like those by Wisse *et al* (2024b) or Silva *et al* (2025), may better preserve signal quality while minimizing cardiovascular interference.

Aiming to optimize breath detection, Cornejo *et al* (2022) used the most dorsal ROI signal for timing of the breathing cycle, with the dorsal ROI being closest to the diaphragm. This approach is simpler than shifting the start of the breathing cycle forward for any pixel starting inflation early, as was described by Adler *et al* (2024). However, it can become problematic if there is no/minimal ventilation distribution toward the most dorsal ROI.

Functional lung segmentation is generally used to remove noise from non-pulmonary structures, often based on a pixel TIV threshold (e.g. 20% (Jiang *et al* 2023) or 10% (Adler *et al* 2024) of maximum impedance change). However, due to the apparent phase shift with pendelluft, pixel TIV within pendelluft-associated regions may be below such threshold, resulting in the unintended removal of those pixels for pendelluft computation, while in fact, they are ventilated (see e.g. Figure 3 upper right corners in recording 2)—this may be even more relevant in situations where low-pass filtering already reduces (pixel) TIV. Sang *et al* (2020) used a threshold based on the pixel standard deviation to reduce the exclusion of delayed regions when using a TIV threshold; however, this may include regions with ringing artifacts. Menga *et al* (2023) determined non-lung regions based on anthropometric data, excluding the heart and chest wall, which should be more accurate (Menga *et al* 2023) but this is only applicable to recordings from the LuMon EIT device. Therefore, this method cannot be applied directly to EIT data collected with a machine from a different vendor. A more advanced lung segmentation method would involve using CT for lung region determination (Yang *et al* 2021). As a solution, we recently developed a novel method for functional lung space selection using the established watershed segmentation method (i.e. Watershed-FLS), where pendelluft-associated pixels are maintained in further analysis (Somhorst *et al* 2026b). Supplemental figure 3 demonstrates this by applying Watershed-FLS to the same dataset of figure 3, recording 2.

The calculation of pendelluft also strongly depends on ROI selection. Some studies divide the lungs into 4 regions (Coppadoro *et al* 2020b, Cornejo *et al* 2022), but such segmentation assumes homogeneity within regions, as well as pendelluft occurring exclusively between large regions, potentially underestimating pendelluft (Coppadoro *et al* 2020b, Lin *et al* 2023). Pixel-by-pixel analysis improves spatial resolution (Sang *et al* 2020) but is more susceptible to noise (Liu *et al* 2024).

Several studies determined pendelluft amplitude using single-breath measurements (Santini *et al* 2019, Cornejo *et al* 2022), whereas others averaged values over multiple breaths (Sang *et al* 2020, Coppadoro *et al* 2020b, Menga *et al* 2023, Adler *et al* 2024). Given the potential variability in pendelluft across breaths, single-breath measurements may not fully capture the phenomenon. Therefore, averaging pendelluft over multiple breaths is a more representative approach. Menga *et al* (2023) however, created an average EIT breath signal first and computed pendelluft for this averaged breath prior to computing pendelluft (Menga *et al* 2023). With unstable breathing patterns and varying respiratory rates or inspiratory times, breath averaging could either introduce phase shift and thus artificially generate pendelluft, or may average out phase differences between regions, leading to potential under- or overestimation of pendelluft which highlights a significant limitation.

4.3. Threshold for pendelluft occurrence

The method of Sang *et al* (2020) is among the most frequently used in pendelluft literature (Chi *et al* 2022, Jiang *et al* 2023, Wang *et al* 2023, Liu *et al* 2024, Xiao *et al* 2024). However, due to its sensitivity because of pixel-level computations, multiple studies established a cut-off value for pendelluft occurrence, for instance when the pendelluft amplitude exceeded 2.5% of the global TIV (Chi *et al* 2022, Liu *et al* 2024). Chi *et al* (2022) established this cut-off using healthy volunteer data and taking the 95th percentile of their pendelluft amplitude above which the occurrence of pendelluft was significant. Xiao *et al* (2024) set a cut-off value of 0.05% of the tidal volume. Considering the nature of pendelluft, it is more appropriate to consider it as a continuous phenomenon, with thresholds mainly serving to define ranges of potential clinical relevance rather that presence/absence. Despite these efforts, universally accepted thresholds for clinically relevant and useable pendelluft values are yet to be established.

4.4. Clinical implications and toward standardization

EIT is currently the only real-time bedside method for pendelluft detection. Bedside pendelluft quantification improves our understanding of lung mechanics in mechanically ventilated patients, especially in the presence of patient effort. Associations have been reported between pendelluft and prolonged mechanical ventilation in patients with a PaO_2/FiO_2 ratio of below 200 mmHg (Chi *et al* 2022), prolonged ICU stays and higher mortality in difficult-to-wean patients (Liu *et al* 2024), and elevated inflammatory markers associated with ventilator-induced lung injury in ARDS patients (Cornejo *et al* 2022).

Despite these associations, the causal pathways, prevalence and clinical significance of pendelluft remains poorly understood. This can partly be explained by the limited generalizability and comparability of studies when different methodologies are used—both in terms of EIT preprocessing and pendelluft computation. In this context, we aligned the unique pendelluft computations methods and propose standardized parameter definitions, allowing comparisons across methods. Aligning these methods was complex due to the absence of a reference standard and the inconsistent reporting across studies, requiring communication with respective authors and highlighting the need for standardized reporting (we recently proposed a reporting checklist for EIT studies (Scaramuzzo *et al* 2024)).

With our work we emphasize the need for methodological consensus to enhance generalizability of studies before interpreting the clinical consequences of pendelluft. In addition, future work is needed to compare the different algorithms when applied to a large and diverse set of clinical EIT data, in order to elucidate the added value of each algorithm and specify which pendelluft features should be reported. For instance, we should consider which methods best differentiate pendelluft values between controlled and spontaneous ventilation modes, as well as between patients with and without lung injury, given the expected increase in pendelluft with greater respiratory effort and more severe lung injury. Cut-off values for clinically relevant pendelluft will also facilitate translation in clinical practice. Methodological standardization can improve clinical use by providing pendelluft reference and cut-off values that, to date, are applicable only if the method and computation are precisely replicated. Standardization should also include proper lung segmentation that is pendelluft-aware, such as with our new Watershed method (Somhorst *et al* 2026b).

All presented algorithms focus on pendelluft that occurs around the start of or during inspiration. However, NIC can occur not only after the start of global or functional inspiration (for pixels still deflating while others are already inflating) but also before the start of global or functional expiration (for pixels already deflating while others are still inflating). Similarly, PIC can occur before the start of global or functional inspiration or after the start of global or functional expiration. For future research and clarity, we propose an integration of this time-dependent measure (see supplemental figure 4).

We contribute to standardization of EIT analyses through our open-source *eitprocessing* software (Somhorst *et al* 2026a) that we made available to the EIT community. In the near future, we will add the pendelluft algorithms as evaluated in the current paper to our repository (Watershed FLS is already available), thereby contributing to transparent, reproducible research on the pendelluft phenomenon. Future research should focus on evaluating whether the different algorithms are redundant or complimentary and which could be most useful, balancing both (bedside) implementation capability (Wisse *et al* 2024a) and clinical value. Since EIT is currently the only noninvasive bedside tool for detecting and quantifying pendelluft, well-validated algorithms and proven clinical relevance will further solidify the usefulness of EIT for monitoring the impact of spontaneous breathing on regional lung mechanics.

5. Conclusion

Different methods for quantifying pendelluft with EIT exist which differ considerably in pendelluft quantification and in EIT preprocessing. Further development and consensus on quantification techniques and standardized reporting are necessary for advancing research into pendelluft and improving clinical applicability. Then, we can investigate the clinical significance of pendelluft and impact on patient outcomes.

Acknowledgment

This study was partially supported by NWO through a personal grant (ZonMw Veni Dr Jonkman, number 09150162210061) paid to the Department of Intensive Care, Erasmus University Medical Center.

Data availability statement

The code that support the findings of this study will be openly available following an embargo at the following URL/DOI: https://github.com/EIT-ALIVE/eitprocessing (Somhorst *et al* 2026a).

Supplemental file 1 available at: https://doi.org/10.1088/1361-6579/ae7d81/data1.

Conflict of interest

AHJ has previously received research grants (paid to the institution) from Pulmotech B. V., Liberate Medical, Health~Holland, Finapres, and the Netherlands eScience Center, all unrelated to this work. Other authors declare no competing interests.

Author contributions

Annemijn H Jonkman 0000-0001-8778-5135
Conceptualization (equal), Data curation (equal), Investigation (equal), Methodology (equal), Resources (equal), Supervision (equal), Writing – original draft (lead), Writing – review & editing (equal)

Juliette E Francovich 0009-0004-0976-5082
Data curation (equal), Investigation (equal), Methodology (equal), Software (lead), Visualization (equal), Writing – review & editing (equal)

Anne Lotte Kuiper 0009-0009-9662-4072
Data curation (equal), Methodology (equal), Software (supporting), Writing – review & editing (equal)

Diederik Gommers 0000-0001-6808-7702
Investigation (equal), Writing – review & editing (equal)

Gaetano Scaramuzzo 0000-0001-9739-4082
Investigation (equal), Methodology (equal), Writing – review & editing (equal)

Peter Somhorst 0000-0003-3490-2080
Conceptualization (equal), Investigation (equal), Methodology (equal), Software (supporting), Supervision (equal), Visualization (lead), Writing – original draft (equal), Writing – review & editing (equal)

References

Adler A, Becher T, Handel C and Frerichs I 2024 Fraction of reverse impedance change (FRIC): a quantitative electrical impedance tomography measure of intrapulmonary pendelluft *Physiol. Meas.* **45** 10NT01

Arellano D H *et al* 2023 Pendelluft in hypoxemic patients resuming spontaneous breathing: proportional modes versus pressure support ventilation *Ann. Intensive Care* **13** 131

Bassi T *et al* 2025 Effect of higher or lower peep on pendelluft during spontaneous breathing efforts in acute hypoxemic respiratory failure *Respir. Care* **70** 126–33

Bello G *et al* 2024 High vs low PEEP in patients with ARDS exhibiting intense inspiratory effort during assisted ventilation: a randomized crossover trial *Chest* **165** 1392–405

Brauer L 1909 Erfahrungen und Überlegungen zur Lungenkollapstherapie *Beiträge zur Klinik der Tuberkulose und spezifischen Tuberkulose-Forschung* **12** 49–154

Chi Y, Zhao Z, Frerichs I, Long Y and He H 2022 Prevalence and prognosis of respiratory pendelluft phenomenon in mechanically ventilated ICU patients with acute respiratory failure: a retrospective cohort study *Ann. Intensive Care* **12** 22

Coppadoro A, Eronia N, Foti G and Bellani G 2020a Event-triggered averaging of electrical impedance tomography (EIT) respiratory waveforms as compared to low-pass filtering for removal of cardiac related impedance changes *J. Clin. Monit. Comput.* **34** 553–8

Coppadoro A, Grassi A, Giovannoni C, Rabboni F, Eronia N, Bronco A, Foti G, Fumagalli R and Bellani G 2020b Occurrence of pendelluft under pressure support ventilation in patients who failed a spontaneous breathing trial: an observational study *Ann. Intensive Care* **10** 39

Cornejo R A *et al* 2022 Inflammatory biomarkers and pendelluft magnitude in ards patients transitioning from controlled to partial support ventilation *Sci. Rep.* **12** 20233

Frerichs I *et al* 2017 Chest electrical impedance tomography examination, data analysis, terminology, clinical use and recommendations: consensus statement of the TRanslational EIT developmeNt stuDy group *Thorax* **72** 83–93

Grieco D L *et al* 2023 Physiological effects of awake prone position in acute hypoxemic respiratory failure *Crit Care* **27** 315

Harada K, Saoyama N, Izumi K, Hamaguchi N, Sasaki M and Inoue K 1983 Experimental pendulum air in the flail chest *Jpn. J. Surg.* **13** 219–26

Heines S J H, de Jongh S A M, de Jongh F H C, Segers R P J, Gilissen K M H, van der Horst I C C, van Bussel B C T and Bergmans D 2024 A novel positive end-expiratory pressure titration using electrical impedance tomography in spontaneously breathing acute respiratory distress syndrome patients on mechanical ventilation: an observational study from the MaastrICCht cohort *J. Clin. Monit. Comput.* **39** 127–39

Jiang H, Han Y, He G, Cui W, Cheng F, Fang Q and Zheng X 2023 Evaluating bronchial anastomotic stenosis dynamically by electrical impedance tomography in a lung transplant recipient: a case report *Ann. Transl. Med.* **11** 222

Lee J H, Kang P, Park J B, Ji S H, Jang Y E, Kim E H, Kim J T and Kim H S 2024 Determination of optimal positive end-expiratory pressure using electrical impedance tomography in infants under general anesthesia: comparison between supine and prone positions *Paediatr. Anaesth.* **34** 758–67

Lin W C, Su P F and Chen C W 2023 Pendelluft in patients with acute respiratory distress syndrome during trigger and reverse triggering breaths *Sci. Rep.* **13** 22143
Liu W, Chi Y, Zhao Y, He H, Long Y and Zhao Z 2024 Occurrence of pendelluft during ventilator weaning with T piece correlated with increased mortality in difficult-to-wean patients *J. Intensive Care* **12** 23
Lowhagen K, Lundin S and Stenqvist O 2010 Regional intratidal gas distribution in acute lung injury and acute respiratory distress syndrome assessed by electric impedance tomography *Minerva Anestesiol.* **76** 1024–35
Maloney J V JR., Schmutzer K J and Raschke E 1961 Paradoxical respiration and "pendelluft" *J. Thorac. Cardiovasc. Surg.* **41** 291–8
Mauri T, Eronia N, Turrini C, Battistini M, Grasselli G, Rona R, Volta C A, Bellani G and Pesenti A 2016 Bedside assessment of the effects of positive end-expiratory pressure on lung inflation and recruitment by the helium dilution technique and electrical impedance tomography *Intensive Care Med.* **42** 1576–87
Menga L S *et al* 2023 Respective effects of helmet pressure support, continuous positive airway pressure, and nasal high-flow in hypoxemic respiratory failure: a randomized crossover clinical trial *Am. J. Respir. Crit. Care Med.* **207** 1310–23
Otis A B, Mckerrow C B, Bartlett R A, Mead J, Mcilroy M B, Selverstone N J and Radford E P 1956 Mechanical factors in distribution of pulmonary ventilation *J. Appl. Physiol.* **8** 427–43
Sang L, Zhao Z, Yun P J, Frerichs I, Moller K, Fu F, Liu X, Zhong N and Li Y 2020 Qualitative and quantitative assessment of pendelluft: a simple method based on electrical impedance tomography *Ann. Transl. Med.* **8** 1216
Santini A, Mauri T, Dalla Corte F, Spinelli E and Pesenti A 2019 Effects of inspiratory flow on lung stress, pendelluft, and ventilation heterogeneity in ARDS: a physiological study *Crit Care* **23** 369
Scaramuzzo G *et al* 2024 Electrical impedance tomography monitoring in adult ICU patients: state-of-the-art, recommendations for standardized acquisition, processing, and clinical use, and future directions *Crit Care* **28** 377
Silva D F, Muders T, Reinartz S, Putensen C and Leonhardt S 2025 Adaptive cardiorespiratory separation with harmonic models and filters: the case of electrical impedance tomography *IEEE Trans. Biomed. Eng.* **72** 3288–99
Somhorst P, Bodor D L, Francovich J, Wisse J J, Baccinelli W and Jonkman A H 2026a eitprocessing: a python package for analysis of electrical impedance tomography data *J. Open Source Softw.* **11** 8179
Somhorst P, Francovich J E, Gommers D and Jonkman A H 2026b Watershed functional lung space: a pendelluft-aware EIT segmentation method *Physiol. Meas.* **47** 02NT01
Tabuchi A, Nickles H T, Kim M, Semple J W, Koch E, Brochard L, Slutsky A S, Pries A R and Kuebler W M 2016 Acute lung injury causes asynchronous alveolar ventilation that can be corrected by individual sighs *Am. J. Respir. Crit. Care Med.* **193** 396–406
Tsuzaki K, Hales C A, Strieder D J and Venegas J G 1993 Regional lung mechanics and gas transport in lungs with inhomogeneous compliance *J. Appl. Physiol.* **75** 206–16
Vyshedskiy A and Murphy R 2012 Pendelluft in chronic obstructive lung disease measured with lung sounds *Pulm. Med.* **2012** 139395
Wang D *et al* 2023 Pendelluft as a predictor of weaning in critically ill patients: an observational cohort study *Front. Physiol.* **14** 1113379
Wisse J J, Scaramuzzo G, Pellegrini M, Heunks L, Piraino T, Somhorst P, Brochard L, Mauri T, Ista E and Jonkman A H 2024a Clinical implementation of advanced respiratory monitoring with esophageal pressure and electrical impedance tomography: results from an international survey and focus group discussion *Intensive Care Med. Exp.* **12** 93
Wisse J J, Somhorst P, Behr J, Van Nieuw Amerongen A R, Gommers D and Jonkman A H 2024b Improved filtering methods to suppress cardiovascular contamination in electrical impedance tomography recordings *Physiol. Meas.* **45** 055010
Xiao Z, Yang L, Dai M, Lu W, Liu F, Frerichs I, Gao C, Sun X and Zhao Z 2024 Regional ventilation distribution before and after laparoscopic lung parenchymal resection *Physiol. Meas.* **45** 015004
Xiao Z, Zhang N, Zhang X, Lu W, Gao C and Sun X 2022 Case report: post-thoracoscopy pendelluft monitoring *Front. Med.* **9** 1108637
Yang L, DAI M, Moller K, Frerichs I, Adler A, Fu F and Zhao Z 2021 Lung regions identified with CT improve the value of global inhomogeneity index measured with electrical impedance tomography *Quant. Imaging Med. Surg.* **11** 1209–19
Yoshida T *et al* 2017 Volume-controlled ventilation does not prevent injurious inflation during spontaneous effort *Am. J. Respir. Crit. Care Med.* **196** 590–601
Yoshida T, Torsani V, Gomes S, De Santis R R, Beraldo M A, Costa E L, Tucci M R, Zin W A, Kavanagh B P and Amato M B 2013 Spontaneous effort causes occult pendelluft during mechanical ventilation *Am. J. Respir. Crit. Care Med.* **188** 1420–7
Zhao Z, Yun P J, Kuo Y L, Fu F, Dai M, Frerichs I and Moller K 2018 Comparison of different functional EIT approaches to quantify tidal ventilation distribution *Physiol. Meas.* **39** 01NT01